Pacific Northwest
NATIONAL LABORATORY

PNNL-39805

Thermodynamics of Tritium Trapping by Point Defects at Interfacial Cr-based Phases of the Al Coating

September 2026

Michel Sassi
David J. Senor
Andrew M. Casella

U.S. DEPARTMENT OF ENERGY

Prepared for the U.S. Department of Energy
under Contract DE-AC05-76RL01830

DISCLAIMER

PACIFIC NORTHWEST NATIONAL LABORATORY
operated by
BATTELLE
for the
UNITED STATES DEPARTMENT OF ENERGY
under Contract DE-AC05-76RL01830

Printed in the United States of America

Available to DOE and DOE contractors from
the Office of Scientific and Technical Information,
P.O. Box 62, Oak Ridge, TN 37831-0062
www.osti.gov
ph: (865) 576-8401
fax: (865) 576-5728
email: reports@osti.gov

Available to the public from the National Technical Information Service
5301 Shawnee Rd., Alexandria, VA 22312
ph: (800) 553-NTIS (6847)
or (703) 605-6000
email: info@ntis.gov
Online ordering: http://www.ntis.gov

PNNL-39805

Thermodynamics of Tritium Trapping by Point Defects at Interfacial Cr-based Phases of the Al Coating

September 2026

Michel Sassi
David J. Senor
Andrew M. Casella

Prepared for
the U.S. Department of Energy
under Contract DE-AC05-76RL01830

Pacific Northwest National Laboratory
Richland, Washington 99352

Summary

Density functional theory (DFT) simulations have been carried out to evaluate the potential for tritium trapping by metal vacancies in four Cr-containing phases (i.e., Cr_3Si, $Al_{0.3}Cr_{0.7}$, Al_8Cr_5-HT, and Al_8Cr_5) identified near the interface between the Al coating and 316 stainless steel (316 SS) cladding. In addition, an *ab initio* thermodynamics approach has been employed to predict the temperature and T_2-partial pressure dependence on the thermodynamics of singly tritiated defects. Key results in this work suggest that metal vacancies in the four phases have the potential to favorably trap tritium species, especially Si vacancies in Cr_3Si phase. This overall thermodynamic trend can be correlated to the energy cost of having an interstitial tritium in the lattice, which has been calculated to range from 0.17 eV in Al_8Cr_5-HT to 0.89 eV in Cr_3Si. A comparison of the results from this study with previous theoretical works investigating tritium behavior in other Fe-Al phases identified in the aluminide coating, suggests that metal vacancies are generally able to trap tritium in various Fe-Al aluminide phases. Especially, it was found that Si and Al vacancies would be the most efficient to trap for tritium, followed by Cr vacancies, then Fe and Ni vacancies. In the four Cr-based material phases investigated in this work, it is interesting to note that, in the absences of Fe or Ni species, strong interactions between tritium and the metal vacancies are always occurring by the formation of preferential Cr—T bonds (i.e., no Si—T or Al—T bonds were formed).

1.0 Introduction

Reports[1,2] have indicated that a small but steady fraction of atomic tritium generated in ^{6}Li enriched γ-$LiAlO_2$ pellets during neutron irradiation permeates out of the TPBAR during production. After a decade of fundamental research, the NNSA supported Tritium Modernization program has provided a much better understanding of irradiation effects on pellet, getter and cladding materials, and has pointed at possible design improvements that have the potential to increase tritium production, improve design margins, or reduce tritium permeation into the WBN coolant.[3] As our understanding improve, many of the studies now seek to explain the mechanisms behind the observed phenomena and an essential first step to develop a mechanistic understanding of tritium behavior in TPBAR components is provided by material characterization. While it has been observed that tritium permeation is slowed due to the aluminide coating, the actual mechanisms for tritium trapping and its trapping locations are still elusive. So far, observations suggest that tritium is trapped "somewhere" in the aluminide coating and not in the 316 SS. However, as shown in Figure 1A and 1B, numerical simulations using density functional theory (DFT) performed by Sassi[4–6] have indicated that tritium would be more efficiently trapped by defects in phases such as $FeNiAl_5$, Fe_4Al_{13}, and $Fe_2Al_{5.6}$ found in the inner-iron aluminide coating, and (Fe, Cr, Ni), $AlFe_3$, NiAl, and AlFe found near the interface between the Al-coating and the 316 SS rather than in the $Al_{12}(TM)_{2.35}$ phase found in the outer-region of the Al-coating located below the Al-oxide phase present at the surface.

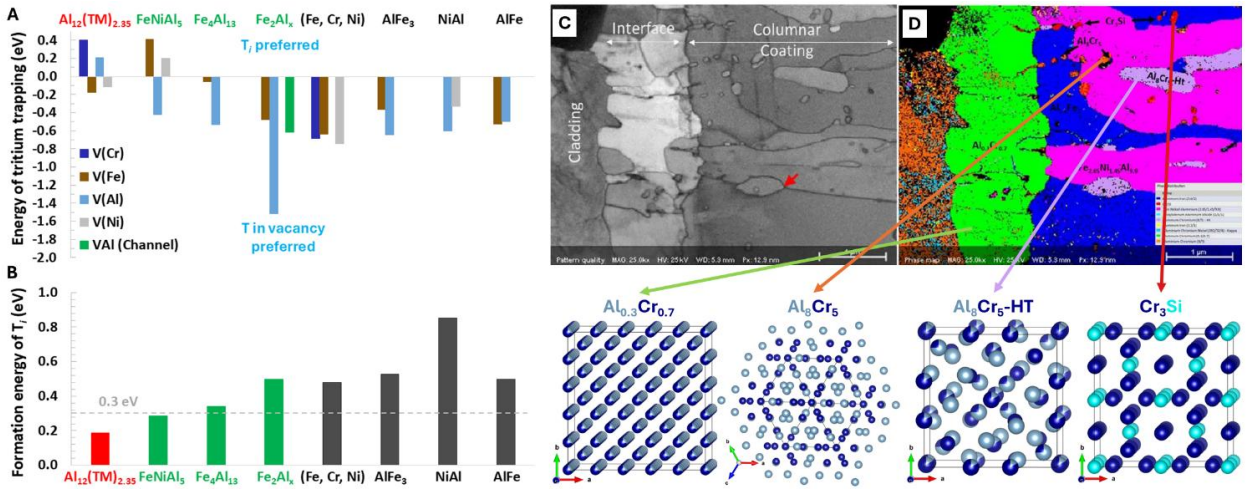

Figure 1: (A) Energy for tritium trapping in the various identified Fe-Al phases of the Al coating. (B) Interstitial tritium binding energy. Grain quality maps (C) and phase map (D) collected at the interface between the 316 SS cladding and aluminide coating collected using t-EBSD.[8]

Key findings of these simulations are that Al vacancies are generally the best trap for tritium, followed by Fe vacancies, then by Ni or Cr vacancies, and that tritium is preferentially binding Fe species rather than Al, Cr, or Ni species. It was also found that there could be a correlation

between interstitial tritium solubility and the effectiveness for trapping by metal vacancies (Figure 1B).

Based on the microscopy imaging conducted by Silverstein *et al.*,[7] Cr-based phases could be identified (Figure 1C and 1D) near the interface between the Al-coating and 316 SS.[8] Interestingly, these phases do not bear Fe in their composition. To provide a deeper understanding of tritium interaction within TPBAR's aluminide coating, we used *ab initio* density functional theory (DFT) simulations to investigate the thermodynamics of tritium trapping by point defects in the Cr-based phases found at the interface between the aluminide coating and 316 SS. The systematic evaluation of trapping effectiveness of the phases identified in the Al-coating can help guide the design of a deposition process to intentionally create phases that maximize tritium trapping. To that end, the findings will be combined with previous theoretical investigations to provide a more complete picture of tritium behavior in complex chemical environments. The work will focus on the following four Cr-based phases, namely Al_8Cr_5, Al_8Cr_5-HT, Cr_3Si, and $Al_{0.3}Cr_{0.7}$.

2.0 Computational Details

DFT calculations have been performed with the VASP code.[9] All the simulations used the generalized gradient approximation (GGA) exchange-correlation as parametrized in the Perdew, Burke, and Ernzerhof (PBE) functional.[10,11] A cutoff energy of 350 eV for the plane-wave basis set has been used and spin-polarization has been taken into account. The simulations of the Cr_3Si (2×2×2 supercell), $Al_{0.3}Cr_{0.7}$ (3×3×3 supercell), and Al_8Cr_5-HT phases used a Brillouin zone sampling at the Γ-point with a *k*-point mesh of 5×5×5. The simulation of hexagonal Al_8Cr_5 phase used a Brillouin zone sampling at the Γ-point with a *k*-point mesh was 4×4×6. In all cases, the total energy was converged with a criterion of 10^{-5} eV/cell. Due to their similar electronic structure, the pseudopotential of standard hydrogen (^{1}H) has been used to describe tritium (^{3}H), however, to account for the isotopic effect, the mass in the pseudopotential has been modified to match that of the isotope atom.

Each of the four phases investigated in this work were first fully relaxed and the optimized lattice parameters of the defect-free phases were in good agreement with their respective experimental values,[12–15] which as shown in Table 1, had an error generally within ~1%.

Phase	a (Å)	b (Å)	c (Å)	α (°)	β (°)	γ (°)
Cr_3Si	*4.555*	*4.555*	*4.555*	*90.0*	*90.0*	*90.0*
	4.507 (-1.05%)	4.507 (-1.05%)	4.507 (-1.05%)	90.0 (0.0%)	90.0 (0.0%)	90.0 (0.0%)
$Al_{0.3}Cr_{0.7}$	*2.960*	*2.960*	*2.960*	*90.0*	*90.0*	*90.0*
	2.950 (-0.32%)	2.943 (-0.59%)	2.936 (-0.81%)	89.86 (-0.15%)	90.13 (0.15%)	90.08 (0.08%)
Al_8Cr_5-HT	*9.090*	*9.090*	*9.090*	*90.0*	*90.0*	*90.0*
	8.997 (-1.02%)	9.036 (-0.59%)	9.020 (-0.77%)	90.04 (0.04%)	90.13 (0.14%)	89.76 (-0.26%)
Al_8Cr_5	*12.718*	*12.718*	*7.937*	*90.0*	*90.0*	*120.0*
	12.693 (-0.20%)	12.683 (-0.20%)	7.904 (-0.42%)	90.0 (0.0%)	90.0 (0.0%)	120.0 (0.0%)

Table 1: Comparison of the experimental (in *italic*) and calculated lattice parameters for the four phases investigated. The errors between calculated and experimental values are provided in brackets.

After introducing interstitial tritium (T_i) and metal vacancy (V(M)) defects, only the atomic coordinates were allowed to relax while the lattice parameters were kept fixed to their relaxed defect-free bulk structures values. Subsequently, tritium loading of the metal vacancy has been investigated by filling it with several tritium atoms. The energy of multiple configurations was evaluated and only the most energetically favorable one at each loading was used for thermodynamic calculations.

To evaluate the relative thermodynamic stability of non-tritiated and tritiated metal vacancies at conditions relevant to in-reactor operation, *ab initio* thermodynamics calculations have been carried out in which the temperature (T) and tritium partial pressure $(p(T_2))$ dependance of the Gibbs free energy of formation of defects, $\Delta G_f(T, p(T_2))$, has been calculated using the following generic equation:

$$\Delta G_f(T, p(\mathrm{T_2})) = (E^T_{\text{defect}} + E^{ZPE}_{\text{defect}} + \Delta\mu(T)_{\text{defect}}) - \left(E^T_{\text{perf}} + E^{ZPE}_{\text{perf}} + \Delta\mu(T)_{\text{perf}}\right) + \sum_i n_i(E^T_i + E^{ZPE}_i + \Delta\mu_i(T, p(\mathrm{T_2}))) \quad (1)$$

where n_i is the number of atoms added/removed of each atomic species i. E^T_i, E^{ZPE}_i, and $\Delta\mu_i(T, p(\mathrm{T_2}))$ are respectively the total DFT energy, the zero-point-energy, and the temperature and T_2 partial pressure dependent chemical potential of each reference species i. In order to account for the temperature effect in the various bulk phases, $\Delta\mu(T)_{\text{defect}}$ and $\Delta\mu(T)_{\text{perf}}$ are the temperature-dependent chemical potential of the system with and without defect (i.e., perfect). All the temperature-dependent chemical potentials have been calculated using the following relation:

$$\Delta\mu(T) = (H(T) - H^{\circ}(298.15)) - TS \quad (2)$$

where $H(T)$ and $H^{\circ}(298.15)$ are the system enthalpy at a temperature T and at T=298.15 K, and S is the entropy. Here, $H(T)$, is the Helmholtz free energy as given by $H(T) = -k_B T \ln(Z)$, where Z is the partition function expressed as implemented in the Phonopy code.[16] The calculated temperature dependence of the chemical potential of tritium has been obtained from previous work.[4] The temperature and T_2 partial pressure dependent chemical potential of molecular T_2 has been calculated as:

$$\Delta\mu_{\mathrm{T_2}}(T, p(\mathrm{T_2})) = \mu_{\mathrm{T_2}}(T^{\circ}, p^{\circ}(\mathrm{T_2})) + k_{\mathrm{B}} T \log\left(\frac{p(\mathrm{T_2})}{p^{\circ}(\mathrm{T_2})}\right) \quad (3)$$

where T° and $p^{\circ}(\mathrm{T_2})$ are the temperature and T_2 partial pressure at standard conditions.

3.0 Results and Discussion

3.1 Atomic model structure of $Al_{0.3}Cr_{0.7}$ and Al_8Cr_5-HT

The experimental CIF files of the $Al_{0.3}Cr_{0.7}$ and Al_8Cr_5-HT phases have sites with partial occupancies. In order to find an atomic model that reproduces the stoichiometry experimentally determined and the random ordering of species distribution in the partially occupied sites, we generated special quasi-random structures (SQS)[17] and evaluated their energies. As shown in Figure 2, 64 SQS structures and 46 SQS structures were generated for $Al_{0.3}Cr_{0.7}$ and Al_8Cr_5-HT respectively. Among the structure generated, we selected the lowest energy structure, as shown by the green dot in Figure 2a and 2b, to investigate the thermodynamic behavior of tritium in each of these two phases.

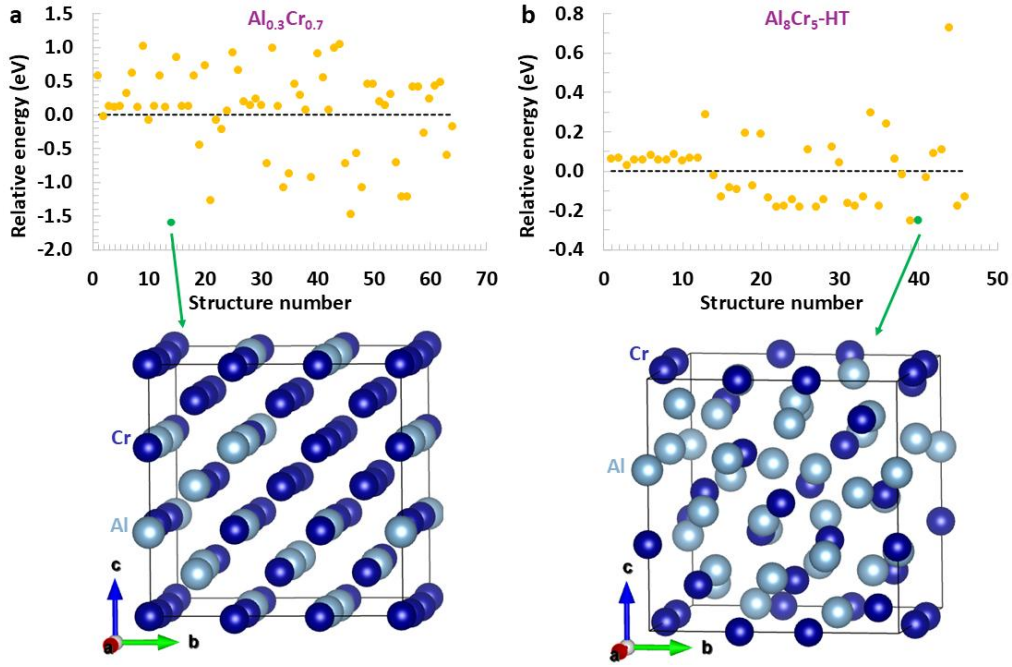

Figure 2: Relative energy of the (a) 64 SQS structures generated for $Al_{0.3}Cr_{0.7}$ and (b) 46 SQS structures generated for Al_8Cr_5-HT phases. The horizontal dashed line represents the average energy of all the SQS structures and has been used as reference.

3.2 Formation energy of metal vacancies in the four interfacial Cr-based phases

We have explored the energy landscape of metal vacancies in each structure and localized the atomic site leading to the lowest vacancy formation energy. As shown in Table 2, which summarizes the formation enthalpy of vacancy calculated for each phase, Cr_3Si has the highest formation energy for Cr species of among all the phases, while the highest formation energy for Al species is obtained for the $Al_{0.3}Cr_{0.7}$ phase. Among all the vacancy formation energies calculated, the one for Si species is the highest of all.

Phase	V_{Cr}	V_{Al}	V_{Si}
Cr_3Si	2.357	0.000	3.847
$Al_{0.3}Cr_{0.7}$	1.693	2.527	0.000
Al_8Cr_5-HT	0.958	1.299	0.000
Al_8Cr_5	1.061	0.866	0.000

Table 2: Calculated formation energies (in eV) of the metal vacancies for the phases of interests.

A comparison of the Gibbs free energy for vacancy formation in each material phase and its temperature dependence is shown in Figure 3. Interestingly, Figure 3 shows that at a temperature of 700 K, Cr vacancies would be easier to create in the materials sharing a similar stoichiometry, Al_8Cr_5-HT phase, followed by the Al vacancies in the Al_8Cr_5 phase.

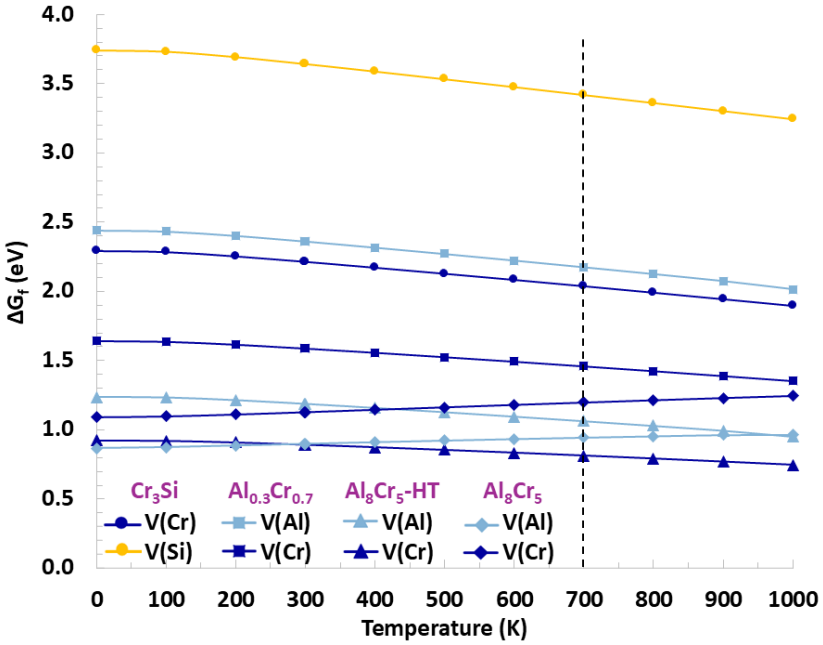

Figure 3: Temperature-dependent Gibbs free energy of formation of metal vacancies in each material phase. The vertical black dashed line helps localize the temperature of in-reactor operation conditions.

3.3 Temperature and T_2-partial pressure dependence of tritiated vacancies

The tritiation of metal vacancies has been performed for up to six tritium atoms. The tritium loading dependent defect energy has been calculated and is plotted in Figure 4 for each material phase. To some degree, adding a tritium species in the vacancy site leads to energetically more stable defects compared to the non-tritiated vacancies. Among the four phases investigated, vacancies in Cr_3Si and $Al_{0.3}Cr_{0.7}$ phases would accommodate the most tritium species, 4 and 3

respectively, while the Cr and Al vacancies in Al_8Cr_5 would favorably accommodate only one tritium species for the Al vacancy and 2 tritium species for the Cr vacancy. For $Al_{0.3}Cr_{0.7}$, Al_8Cr_5-HT, and Al_8Cr_5 it is found that Cr vacancies would accommodate at least as much, or more, tritium species than Al vacancies.

While exploring different tritium configurations in the vacancy space, we noticed that the energetically most favorable and common configurations obtained are those when tritium is bound to a Cr species. As shown by the image inserts in Figure 4, the formation of Cr—T bonds have always been preferred over the formation of Al—T or Si—T bonds. Along with previous theoretical results, this suggests that in the absence of Fe in the material phase, Cr is the next competitive species to help trap tritium by forming bonds.

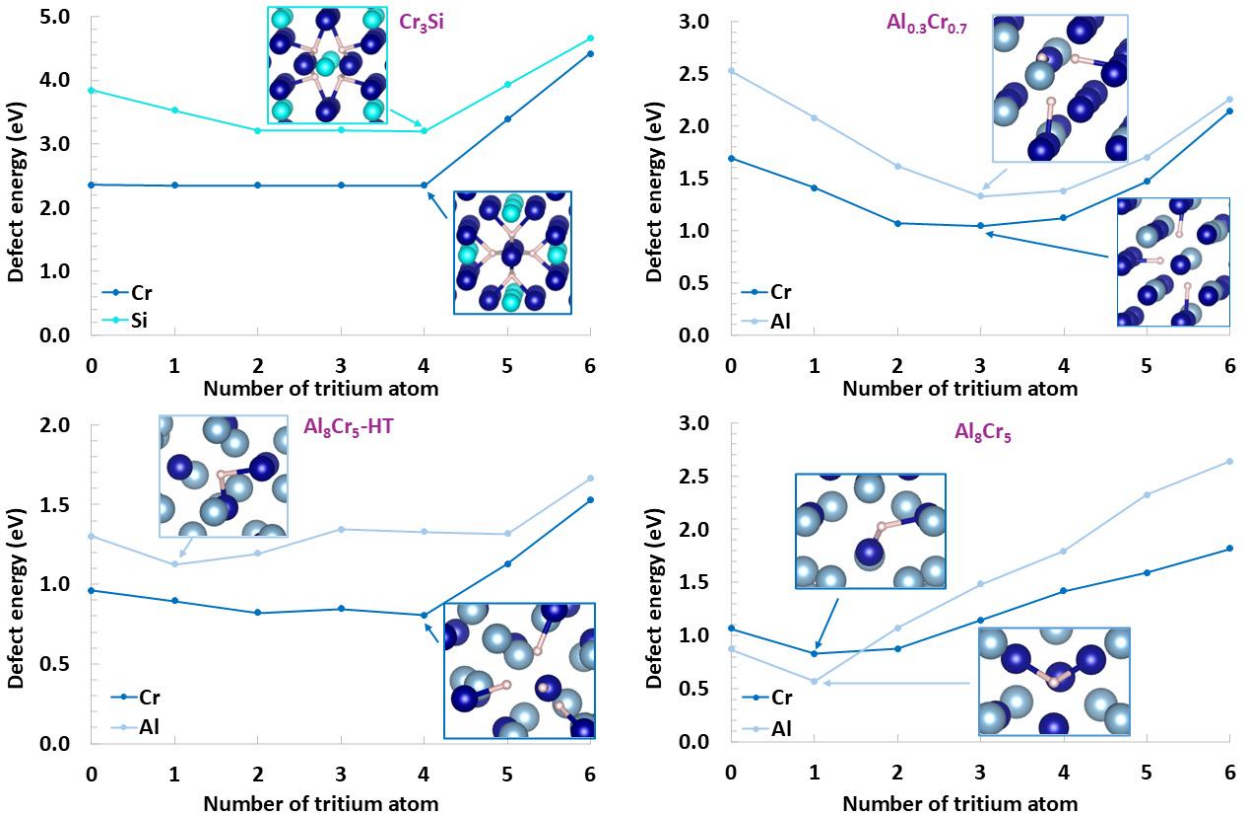

Figure 4: Calculated defect formation energy as a function of tritium loading in metal vacancies.

In order to investigate the effect of temperature and tritium partial pressure ($p(T_2)$) on the relative thermodynamic stability of singly-tritiated and non-tritiated metal vacancies, *ab initio* thermodynamic calculations have been performed. This allows the calculation of the Gibbs free energy of defects at conditions relevant to in-reactor operation, which are a temperature of ~700 K and tritium partial pressures ranging from 10^{-6} to 10^{2} mbar.[18]

An overview of the thermodynamics for the 1st tritiation of metal vacancies in the four interfacial phases is shown in Figure 5. In Figure 5, the purple area highlights the tritium partial

pressure of relevance to TPBAR. Focusing on the range of $p(T_2)$ relevant to in-reactor conditions, Figure 5 shows that none of the tritiated vacancies become more energetically favorable than their respective non-tritiated vacancies. This indicates that regardless of the T_2-partial pressure, the addition of tritium in a vacancy will always be thermodynamically unfavorable. However, these results should also be put in correlation with the energy cost of having an interstitial tritium species in the lattice.

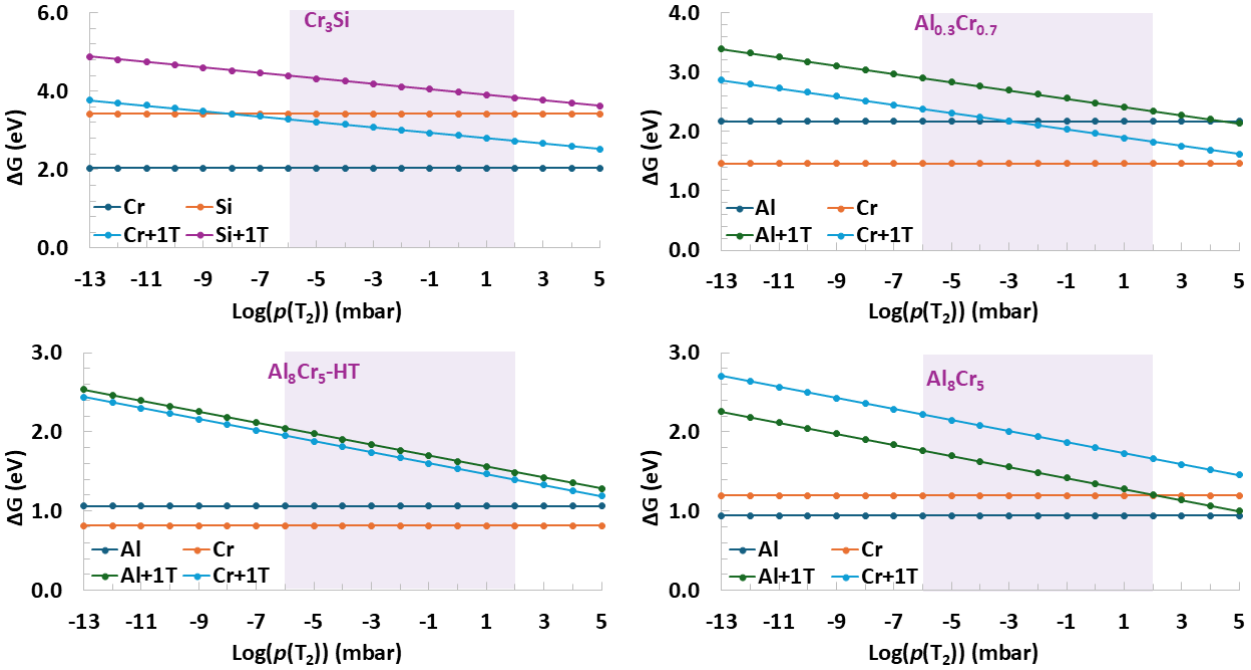

Figure 5: Gibbs free energy of non-tritiated and singly-tritiated metal vacancies as function of tritium partial pressure ($p(T_2)$) at a temperature of 700 K. The purple area highlights the range of tritium partial pressure of interest.

3.4 Trapping potential of metal vacancies

We estimate the trapping efficiency of metal vacancies by comparing the energy of a singly-tritiated vacancy with the energy of an interstitial tritium (T_i) and a non-tritiated vacancy, non-interacting with each other. The trapping enthalpy is calculated using the following relation:

$$\Delta H_{\text{trap}} = E_{\text{V(M)+1T}} - (E_{\text{V(M)}} + 1E_{\text{T}_i}) \qquad (4)$$

With this formulation, a positive enthalpy value indicates that tritium is more favorable as an interstitial species, while a negative energy value suggests that tritium prefers to bind with a metal vacancy. As shown in Figure 6a, for all the vacancies and all four material phases, the

energy of tritium trapping is negative, indicating that in all cases tritium prefers to bind to a metal vacancy rather than remain as an interstitial tritium in the lattice. While it is not thermodynamically favorable to tritiate a vacancy, relative to non-tritiated vacancy, it is still thermodynamically more favorable than having an interstitial tritium.

While many factors can play a role in trapping efficiency, we find that the trapping trend is mostly affected by the formation energy of interstitial tritium, which is shown in Figure 6b, rather than the formation energy of the metal vacancy. More the energy of having an interstitial tritium is high and more metal vacancy trapping would be preferred.

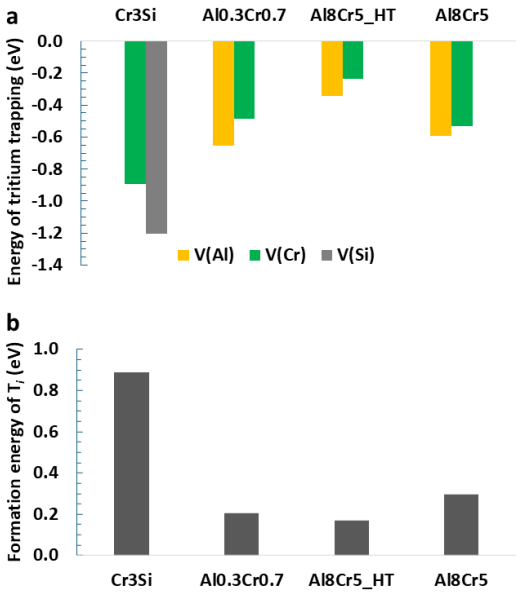

Figure 6: Comparison of tritium trapping potential for the four interfacial Cr-based phases. (a) Energy of trapping tritium in a metal vacancy. (b) Formation energy of interstitial tritium.

3.5 Comparison of tritium trapping efficiency for various phases in Al coating

Based on the STEM imaging conducted by Olszta *et al.*,[19] multiple regions can be distinguished in the aluminide coating: (*i*) surface, (*ii*) outer-iron aluminide, (*iii*) inner-iron aluminide, and (*iv*) interface with 316 SS, with each region having a different set of Fe-Al phases. In previous projects, numerical simulations have investigated both the kinetics of interstitial tritium[20,21] and its thermodynamic behavior[4–6] in Fe-Al phases found in the outer- and inner-iron aluminide coating, and the interface. Key results are that interstitial tritium would diffuse similarly in all the Fe-Al phases identified and that some phases can more effectively trap tritium while others are not efficient for trapping. It was also found that there could be a correlation between interstitial tritium solubility and the efficiency for trapping by metal vacancies (Figure 1A and 1B), that is, if the insertion of an interstitial tritium in a phase costs more than 0.3 eV (empirically determined), then trapping by metal vacancies should be preferred.

The theoretical results currently available informing about the thermodynamic of tritium in the various phases of the Al coating have been combined and compiled in Figure 7. As shown Figure 7, the strongest vacancy traps are obtained for Fe_2Al_x and Cr_3Si phases. However, the overall average (white diamond symbols right panel) for the trapping efficiency for each material phases indicates that the phases at the interface would be more likely to trap tritium species, followed by those present at the inner-aluminide region, then at the outer aluminide region.

The bottom panel in Figure 7 shows the trapping efficiency of each metal vacancy species averaged across the different material phases. The trend is clear; Si vacancies and Al channel (non-lattice Al site of Fe_2Al_x phases) vacancies are the most efficient tritium traps. Then lattice site Al vacancies and Cr vacancies are the second most efficient tritium traps, followed by the Fe and Ni vacancies, which are the weakest trap for tritium.

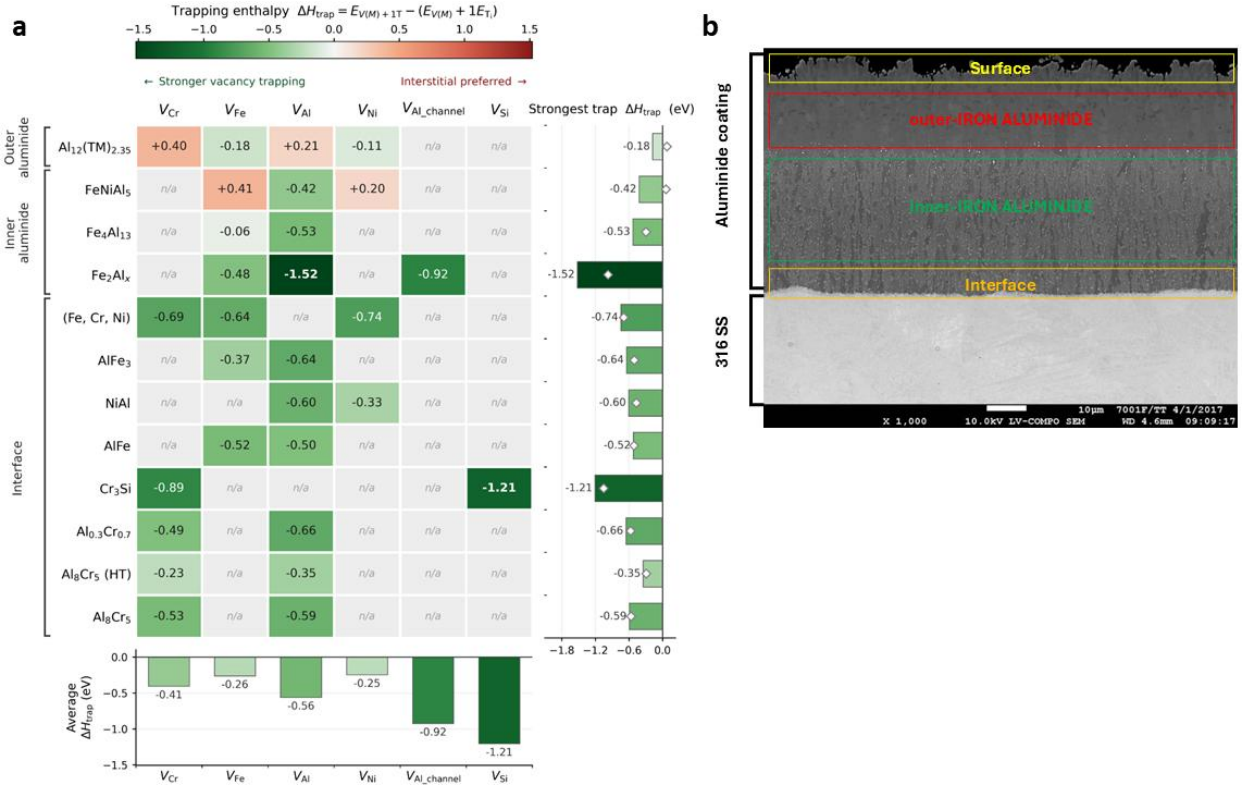

Figure 7: (a) Trapping enthalpy heatmap for six vacancy types across twelve phases, ordered from the outer-aluminide through the inner-aluminide to the interface of the aluminide coating. Positive (red) values indicate a preference for interstitial tritium. Negative (green) values indicate a preference for trapping by metal vacancies. Right panel shows the deepest trap of each phase along with the row average shown by white diamonds symbols. Bottom panel shows the average Δ*H* per vacancy type over the phases in which it exists. (b) STEM image of the aluminide coating and 316 SS highlighting the four regions, adapted from [19].

Conclusion

Density functional theory simulations have been carried out to evaluate the efficiency for tritium trapping by metal vacancies in several phases found in the Al coating. The combined thermodynamic (at 0 K) analysis of 14 phases indicated that Si and Al vacancies, followed Cr, then Fe and Ni vacancies were the most efficient traps for tritium species. A good mechanism for tritium trapping is by the formation of strong Fe—T bonds or Cr—T bonds if Fe is absent from the material composition which are energetically preferable to Ni—T or Al—T bonds. This trend has been theoretically obtained across the range of phases investigated. Altogether, while tritium interacts differently with each phase, the study shows that tritium trapping and retention could be more efficient if metal defects, in particular Al vacancies, are present and if the solubility of interstitial tritium in the different phases is low, thereby, providing a thermodynamic driving force for tritium being bound to metal vacancies.

Acknowledgments

This research was supported by the National Nuclear Security Administration (NNSA) of the U.S. Department of Energy (DOE) through the Tritium Science Research Supporting the Tritium Modernization Program (TMP) managed by Pacific Northwest National Laboratory (PNNL). The authors thank PNNL Research Computing for providing computational resources.

4.0 References

(1) Senor, D. *Science and Technology in Support of the Tritium Modernization Program*; PNNL-31479; Pacific Northwest National Laboratory: Richland, WA, 2021.

(2) *National Nuclear Security Administration Needs to Ensure Continued Availability of Tritium for the Weapons Stockpile*; Report GAO-11-100 Nuclear Weapons; U.S. Government Accountability Office, 2010. https://www.gao.gov/products/gao-11-100

(3) Senor, D. *A Summary of Results from the Tritium Science Competitive Solicitation: FY15 through FY24*; PNNL-38080; Pacific Northwest National Laboratory: Richland, WA, 2025.

(4) Sassi, M.; Chaka, A.; Senor, D.; Casella, A. *First-Principles Study of Tritium Trapping by Point Defects in Fe-Al Aluminide Coating Phases*; PNNL-33519; Pacific Northwest National Laboratory: Richland, WA, 2022. https://doi.org/10.2172/1986035

(5) Sassi, M.; Senor, D. J.; Casella, A. M. *Thermodynamics of Tritium Trapping by Point Defects in Intermetallic Al12(TM)2.35 Aluminide Coating Phase*; PNNL-36641; Pacific Northwest National Laboratory: Richland, WA, 2024.

(6) Sassi, M.; Senor, D. J.; Casella, A. M. *Tritium Trapping Thermodynamics by Point Defects at Interfacial Fe-Al Phases of the Aluminide Coating*; PNNL-38382; Pacific Northwest National Laboratory: Richland, WA, 2025.

(7) Silverstein, J.; Yano, K. *Transmission Kikuchi Diffraction And Transmission Electron Microscopy Characterization Of Aluminide Coatings For TPBAR*; TRIT-T-WP-009 Revision 0; Pacific Northwest National Laboratory: Richland, WA, 2025.

(8) Canfield, N. L.; Johnson, B. R. *Sample Preparation And Analysis Of Unirradiated TPBAR Coated Cladding*; TTP-8-012 Revision 0; Pacific Northwest National Laboratory: Richland, WA, 2018.

(9) Kresse, G.; Furthmüller, J. Efficient Iterative Schemes for *Ab Initio* Total-Energy Calculations Using a Plane-Wave Basis Set. *Phys. Rev. B* **1996**, *54* (16), 11169–11186. https://doi.org/10.1103/PhysRevB.54.11169

(10) Perdew, J. P.; Burke, K.; Ernzerhof, M. Generalized Gradient Approximation Made Simple. *Phys. Rev. Lett.* **1996**, *77* (18), 3865–3868. https://doi.org/10.1103/PhysRevLett.77.3865

(11) Perdew, J. P.; Burke, K.; Ernzerhof, M. Generalized Gradient Approximation Made Simple [Phys. Rev. Lett. 77, 3865 (1996)]. *Phys. Rev. Lett.* **1997**, *78* (7), 1396–1396. https://doi.org/10.1103/PhysRevLett.78.1396

(12) Boren, B. Röntgenuntersuchung der Legierungen von Sili- cium mit Chrom, Mangan, Kobalt und Nickel. *Ark. Kemi Mineral. Och Geol.* **1933**, *A11*, 1–28.

(13) Chakrabarti, D. J.; Beck, P. A. Transport Properties of Cr−Al Solid Solutions. *J. Phys. Chem. Solids* **1971**, *32* (7), 1609–1615. https://doi.org/10.1016/S0022-3697(71)80054-9

(14) Braun, J.; Ellner, M.; Predel, B. Zur Struktur der Hochtemperaturphase Cr5Al8(h). **1992**, *183*, 444–448. https://doi.org/10.1016/0925-8388(92)90766-3

(15) Bradley, A. J.; Lu, S. S. The Crystal Structures of Cr2Al and Cr5Al8. *Z. Für Krist. - Cryst. Mater.* **1937**, *96* (1–6), 20–37. https://doi.org/10.1524/zkri.1937.96.1.20

(16) Togo, A.; Tanaka, I. First Principles Phonon Calculations in Materials Science. *Scr. Mater.* **2015**, *108*, 1–5. https://doi.org/10.1016/j.scriptamat.2015.07.021

(17) Gehringer, D.; Friák, M.; Holec, D. Models of Configurationally-Complex Alloys Made Simple. *Comput. Phys. Commun.* **2023**, *286*, 108664. https://doi.org/10.1016/j.cpc.2023.108664

(18) Luscher, W. G.; Senor, D. J.; Clayton, K. K.; Longhurst, G. R. In Situ Measurement of Tritium Permeation through Stainless Steel. *J. Nucl. Mater.* **2013**, *437* (1–3), 373–379. https://doi.org/10.1016/j.jnucmat.2013.02.009

(19) Olszta, M. J.; Casella, A.; Evarts, J.; Chaka, A.; Sassi, M.; Bowden, M. Surface Microstructure of Aluminide Coatings Formed via Pack Cementation for Tritium Retention. *J. Alloys Compd.* **2026**, *1057*, 186065. https://doi.org/10.1016/j.jallcom.2026.186065

(20) Sassi, M.; Senor, D. J.; Casella, A. M. *Ab Initio* Simulations of Tritium Diffusion in Al-Rich Iron Aluminide Coating Phases. *J. Phys. Chem. C* **2023**, *127* (21), 10315–10323. https://doi.org/10.1021/acs.jpcc.3c01028

(21) Sassi, M.; Senor, D.; Casella, A. *Ab Initio Simulations of Tritium Diffusion in Al2O and Intermetallic Al12(TM)2.34 Aluminide Coating Phases*; PNNL-34818; Pacific Northwest National Laboratory: Richland, WA, 2023. https://doi.org/10.2172/2001006

Pacific Northwest National Laboratory

902 Battelle Boulevard
P.O. Box 999
Richland, WA 99354
1-888-375-PNNL (7665)

www.pnnl.gov